Lamboley et al., http://www.jgp.org/cgi/content/full/jgp.201411250/DC1

Section1: Summary of divalent-ion and proton binding to BAPTA and EGTA

This section starts with a review of relationships for proton and divalent binding to the Ca^{2+} chelators EGTA and BAPTA (most of which is also described in Pape et al., 1995, and Harrison and Bers, 1987). In both cases, the Ca^{2+} chelation site has four carboxyl groups in close proximity (Tsien, 1980). The four groups can bind protons with decreasing affinities as the number of protons already bound increases. The reaction schemes for binding of the first and second protons are given, respectively, by

$$H^+ + X^{4-} \leftrightarrow HX^{3-} \tag{S1}$$

and

$$H^+ + HX^{3-} \leftrightarrow H_2X^{2-}, \tag{S2}$$

where X, for purposes of this study, is either EGTA or BAPTA. At equilibrium, the fraction of divalent-free chelator with one and two protons bound, f_1 and f_2, respectively, are given by

$$f_1 \equiv \frac{\left[HX^{3-}\right]}{[X]} = \frac{10^{pK_1 - pH}}{1 + 10^{pK_1 - pH} + 10^{pK_1 + pK_2 - 2pH}} \tag{S3}$$

and

$$f_2 \equiv \frac{\left[H_2X^{2-}\right]}{[X]} = \frac{10^{pK_1 + pK_2 - 2pH}}{1 + 10^{pK_1 - pH} + 10^{pK_1 + pK_2 - 2pH}}, \tag{S4}$$

where [X] is the sum of concentrations of the divalent-free forms, i.e.,

$$[X] = \left[X^{4-}\right] + \left[HX^{3-}\right] + \left[H_2X^{2-}\right], \tag{S5}$$

and pK_1 and pK_2 are the pKa values for the binding of the first and second protons, respectively. (A pKa value is $-\log_{10}$ of the K_d of the associated proton-binding reaction.) The fraction of divalent-free chelator that is also proton free, f_0, is given by

$$f_0 = 1 - f_1 - f_2 = \frac{1}{1 + 10^{pK_1 - pH} + 10^{pK_1 + pK_2 - 2pH}}. \tag{S6}$$

For both BAPTA and EGTA, the values of pK_3 and pK_4 are very low, so that the forms with three and four protons bound can be neglected for the range of pH values for results in this study (pH ≥6). (All results in this study were obtained at pH 8, except those with BAPTA shown in Fig. S1 in the next section, which includes results from pH 6.0–8.) All of the binding constants given below were measured—or were interpolated to give values—at room temperature (near 22°C) with physiological ionic strength (100–200 mM). For EGTA, the values of 9.48 and 8.81 for pK_1 and pK_2, respectively, were obtained from the tabulated stability constants in Godt and Lindley (1982). With these values of pK_1 and pK_2, the values of f_0, f_1, and f_2 for EGTA at pH 8.0 are 0.0044, 0.1335, and 0.8621. For BAPTA, titration experiments of Tsien (1980) gave values of 6.36 and 5.47 for pK_1 and pK_2, respectively (100 mM KCl; 22 ± 2°C). With these values, the fractional values of $BAPTA^{4-}$, $HBAPTA^{3-}$, and H_2BAPTA^{2-} (f_0, f_1, and f_2) are, respectively, 0.252, 0.577, and 0.171 at pH 6; 0.809, 0.185, and 0.005 at pH 7; and 0.978, 0.022, and 6.6×10^{-5} at pH 8. The main reasons for choosing pH 8.0 for the usual measurement solution was to minimize the protonated forms of BAPTA and to increase the affinity of EGTA for Ca^{2+} (see below), which is important for the step in the method in which EGTA displaces Ca from BAPTA.

The combination of divalent (denoted "Dv^{2+}," where Dv^{2+} could be either Ca^{2+} or Mg^{2+} in this case) with the three forms of divalent-free chelator above are given by the reactions

$$Dv^{2+} + X^{4-} \xleftrightarrow{K_D} DvX^{2-}, \tag{S7}$$

$$Dv^{2+} + HX^{3-} \xleftrightarrow{K_D'} DvX^{2-} + H^+, \tag{S8}$$

and

$$Dv^{2+} + H_2X^{2-} \xleftrightarrow{K_D''} DvX^{2-} + 2H^+. \tag{S9}$$

(The K_d for each of the reactions is shown above the connecting symbol.)

Using the equilibrium relationships above for the divalent-free forms of the chelators, it is readily shown that these three reactions at equilibrium can be combined to give the reaction

$$Dv^{2+} + X \xleftrightarrow{K'_{Dapp,Dv}} DvX^{2-}, \tag{S10}$$

where

$$K'_{Dapp,Dv} = K_D\left(1 + 10^{pK_1 - pH} + 10^{pK_1 + pK_2 - 2pH}\right) \tag{S11}$$

and the associated equilibrium relationship is given by

$$\frac{[DvX^{2-}]}{[X]} = \frac{[Dv^{2+}]}{K'_{Dapp,Dv}}. \tag{S12}$$

As above, $[X]$ is the sum of concentrations of the divalent-free forms. (Note that Eq. S10 is the same as Eq. A9

in Pape et al., 1995, except that $K'_{Dapp,Dv}$ replaces K_{Dapp} for Ca.) The prime symbol in $K'_{Dapp,Dv}$ indicates that the apparent K_d is restricted to the case that only one divalent is present. It is readily shown that in the presence of both Ca^{2+} and Mg^{2+}, the fraction of total chelator occupied by Ca (f_{Ca}) is given by

$$f_{Ca} = \frac{[Ca^{2+}]}{[Ca^{2+}] + K_{Dapp,Ca}}, \quad \text{(S13)}$$

where the apparent K_d for Ca binding to the chelator is given by

$$K_{Dapp,Ca} = K'_{Dapp,Ca}\left(1 + [Mg^{2+}] \Big/ K'_{Dapp,Mg}\right). \quad \text{(S14)}$$

Likewise, the fraction of total chelator occupied by Mg is given by

$$f_{Mg} = \frac{[Mg^{2+}]}{[Mg^{2+}] + K_{Dapp,Mg}}, \quad \text{(S15)}$$

where the apparent K_d for Mg binding to chelator X is given by

$$K_{Dapp,Mg} = K'_{Dapp,Mg}\left(1 + [Ca^{2+}] \Big/ K'_{Dapp,Ca}\right). \quad \text{(S16)}$$

The fraction of chelator in the divalent-free form is given by $1 - f_{Ca} - f_{Mg}$, and the fractions of divalent-free chelator in nonprotonated, singly protonated, and doubly protonated forms (f_0, f_1, and f_2, respectively) are given, respectively, by Eqs. S6, S3, and S4.

Determination of the apparent affinities for Mg and Ca binding to EGTA and BAPTA with Eq. S11 requires values for their associated K_d values (the K_ds with no protons present). For EGTA, values assumed for the K_ds of Ca and Mg were 1.13×10^{-11} M and 6.173×10^{-6} M, respectively (from Godt and Lindley, 1982). With the values of pK_1 and pK_2 for EGTA, the corresponding values for $K'_{Dapp,Ca}$ and $K'_{Dapp,Mg}$ at pH 8.00 for EGTA are 0.00256 and 1,400 µM, respectively. The value of 0.215 µM assumed for the K_d for Ca binding to BAPTA was calculated with Eq. S11 to give the value of 0.22 µM for $K'_{Dapp,Ca}$ at pH 8.00 determined with Fig. 1 in the main text. The value of 16,100 µM assumed for the K_d for Mg binding to BAPTA was calculated with Eq. S11 to give the value of 17,000 µM for $K'_{Dapp,Mg}$ at pH 7.60 reported by Tsien (1980). With the values of pK_1 and pK_2 for BAPTA, the corresponding values for $K'_{Dapp,Ca}$ and $K'_{Dapp,Mg}$ at pH 8.00 for BAPTA are 0.220 and 16,500 µM, respectively.

In summary, this section gives all of the relationships needed to calculate all of the forms of EGTA and BAPTA present in nonnegligible concentrations for the conditions in this study.

Section 2: Absorbance spectra of BAPTA at different pH values

Fig. S1 A plots UV absorbance spectra for divalent-free BAPTA at pH 6, 7, and 8, and another spectrum at pH 8.0 with Ca added to the solution to give a concentration of 1 mM Ca (22.5°C; 120 mM KCl, 2 mM HEPES, and nominal concentration of 0.15 mM for BAPTA; absorbance values were corrected for the slight dilution associated with adjusting pH and adding Ca).Consistent with the observation of Tsien (1980) that there was "very little effect on the spectrum until the pH drops below 6.5 or so," the spectrum at pH 7.0 is very close to that at pH 8.

Fig. S1 B shows five difference spectra derived from the spectra in A. The solid curve (labeled 1) shows the difference spectrum for Ca binding to essentially all of the BAPTA that was present (the 0-Ca curve used for the difference is the pH 8 data shown in A). The dot–dash curve (curve indicated with arrow; because of limited space, the label "2" is not shown) gives the difference between the spectra at pH 8.0 and that at pH 7.0, and the dashed curve gives the difference between

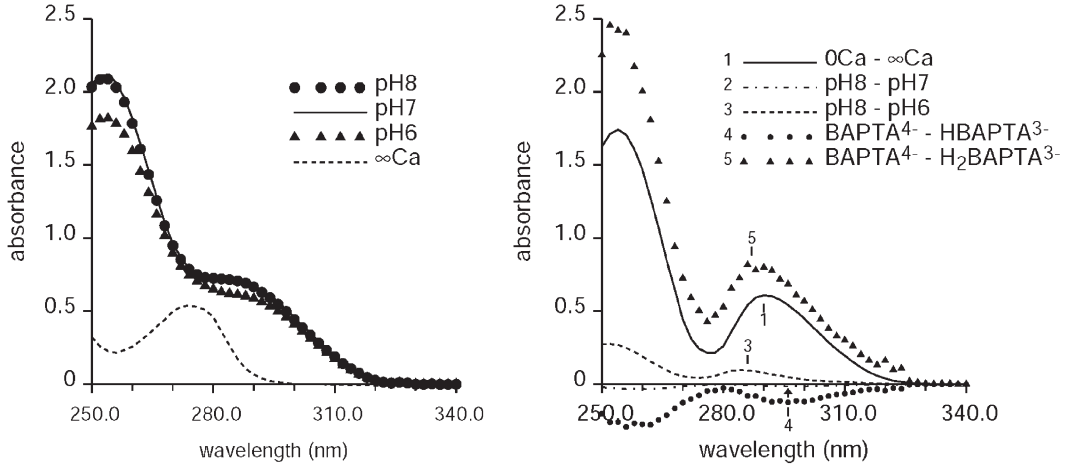

Figure S1. Effects of pH on the absorbance spectra of BAPTA. See text for details.

the spectra at pH 8.0 and pH 6.0 (curve 3). To aid in comparisons with the difference spectrum with Ca binding (curve 1), the difference spectra with binding of one or two protons were calculated as described here. An absorbance spectrum of BAPTA at a particular pH and with no divalent present—like those in A (excluding the curve with Ca present)—should be made up of the sum of absorbance spectra of the different forms of divalent-free BAPTA, as given by the following relationship:

$$A(pH) = A_0 \cdot f_0(pH) + A_1 \cdot f_1(pH) + A_2 \cdot f_2(pH). \quad \text{(S17)}$$

A_0, A_1, and A_2 are the absorbance spectra if all of the BAPTA was bound, respectively, with 0, one, or two protons. The three forms of Eq. S17 corresponding to the three measured spectra (three pH levels in Fig. S1 A) give a set of three linear equations that can be used to solve for the three unknown spectra (A_0, A_1, and A_2) in the usual way, using the values of f_0, f_1, and f_2 for the three pH levels given in the preceding section. The difference spectrum expected if all of the BAPTA was initially present in the singly protonated form and it all became converted to the proton-free form is given by $A_0 - A_1$ and is plotted as closed circles (curve 4) in Fig. S1 B. Interestingly, this has the opposite sign for the difference spectrum going from the Ca-bound to Ca-free form (curve 1). Likewise, the closed triangles give $A_0 - A_2$ (curve 5), the spectrum for conversion between H_2BAPTA^{2-} and $BAPTA^{4-}$. Although this difference spectrum is greater than that of the difference spectrum with Ca removal from BAPTA (curve 1), the two are quite similar. Moreover, because a relatively small error (such as a small error in the scaling factors used to correct for dilution of BAPTA that occurred when adjusting the pH of the solution) would have a relatively large effect on the magnitude of the derived difference spectra, it seems reasonable to suppose that the difference is caused by such an error, and that the binding of two protons to $BAPTA^{4-}$ has about the same effect on the absorbance spectrum as Ca binding.

As discussed in Tsien (1980), BAPTA is composed of the combination of two identical halves, with each half containing an amine group composed of a nitrogen attached to a benzene ring and two carboxylic acid groups, and most of the UV absorbance in the wavelength range of interest of the $BAPTA^{4-}$ form arises from the conjugation between the amine and benzene ring. Tsien (1980) attributed the large absorbance change upon Ca binding to the loss of this conjugation caused by twisting of the nitrogen-benzene ring bonds when the BAPTA molecule rearranges itself to accommodate Ca^{2+} in the chelation pocket formed by the four carboxyl groups. Tsien (1980) proposed that the similarity of the effect of proton binding to BAPTA to that of Ca^{2+} binding was caused by loss of the amine-benzene ring conjugation when a proton binds to the amine group. This explanation, however, does not explain the relative lack of effect on the difference spectrum when only one proton binds and the observation here that the absorbance change was in the opposite direction to that associated with Ca binding (curve 4 vs. curve 1 in Fig. S1 B). If proton binding to the amine group was correct, the expected difference spectrum should have been about half that associated with Ca binding. A more likely explanation is that the first proton binds to one of the carboxyl groups somehow helping with the conjugation between the amine and benzene ring. With two protons bound, an energetically favorable chelation pocket forms (similar to that with Ca bound) with hydrogen bonds linking the four reoriented carboxyl groups, again disrupting the amine-benzene ring conjugation in both halves of the BAPTA molecule. (We wish to acknowledge and thank Marc-André Bonin for suggesting this explanation.)

For the purpose of the experiments in this study (performed at pH 8), the reason for examining the effect of pH on BAPTA absorbance was to assess absorbance changes arising from changes of concentration of proton-bound BAPTA when adding EGTA or Ca standard (changes that would be attributed to changes in the Ca-bound form of BAPTA). Contribution from the doubly protonated form, H_2BAPTA^{2-} can be neglected, as <1 in 10^4 divalent-free BAPTA molecules are present as H_2BAPTA^{2-} at pH 8.0 (previous section). Changes in the contribution of the singly protonated form are expected to be almost negligible because of the calculation in the preceding section showing that only 0.022 of the divalent-free BAPTA is present as $HBAPTA^{3-}$ at pH 8.0, and because the fractional change in $HBAPTA^{3-}$ from the A_M to the A_0 aliquot would be severalfold <0.022, and because the results in Fig. S1 B indicate a relatively small difference in absorbance between the $HBAPTA^{3-}$ and $BAPTA^{4-}$ forms (compare curves 4 and 1).

Section 3: Deviation between measured and actual absorbance caused by stray light

For a substance known to obey Beer's law measured with an ideal spectrophotometer, the reported absorbance versus concentration relationship should be linear. As shown in this section, the spectrophotometer used in this study displayed a significant variation from this ideal behavior, a result attributable to stray light. Stray light in this context appears as an added light intensity (denoted "I_S") recorded by the detector, either from light that doesn't pass through the sample or from light at wavelengths outside of the range nominally set by the spectrophotometer's monochronometer. Evidence (not depicted) indicates that the latter is the case for the spectrophotometer used in this study (Pharmacia Ultraspec 2000). This section shows how the stray

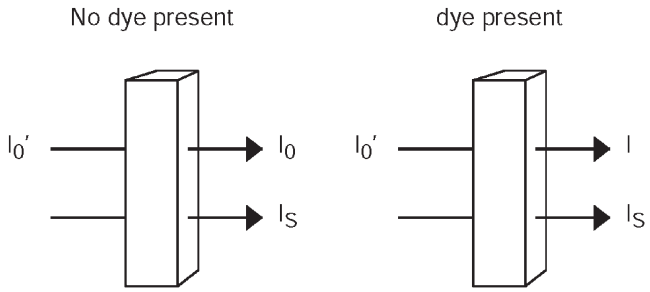

Figure S2. Schematics illustrating the components of light used to determine the absorbance of a substance in a cuvette and the unwanted stray light that is not absorbed. See text for details.

light component was assessed, and how measured absorbance values were corrected to give the true absorbance of the substance(s) of interest in the sample.

With the light intensities depicted in Fig. S2 and defined below, the measured absorbance of the blank and raw absorbance of the sample are given, respectively, by

$$A_{blank} = \log_{10}\left(\frac{I_0^{'} + I_S}{I_0 + I_S}\right) \tag{S18}$$

and

$$A_{raw\_sample} = \log_{10}\left(\frac{I_0^{'} + I_S}{I + I_S}\right), \tag{S19}$$

where $I_0^{'}$ is the intensity of incident, absorbable light and I_0 and I are the intensities of absorbable light leaving the blank (cuvette with water or solution only) and sample, respectively, all at the nominal wavelength set by the monochronometer. The blank-corrected absorbance, denoted "A_{sample}," is given by the difference between A_{raw_sample} and A_{blank}, yielding the relationship

$$A_{sample} = \log_{10}\left(\frac{I_0 + I_S}{I + I_S}\right). \tag{S20}$$

The true absorbance (denoted "A_{true}")—the value sought, i.e., the absorbance attributable to substances in the sample not present in the blank—is given by

$$A_{true} = \log_{10}\left(\frac{I_0}{I}\right). \tag{S21}$$

In general, A_{true} could include the sum of absorbances from several components. In the case of an absorbance

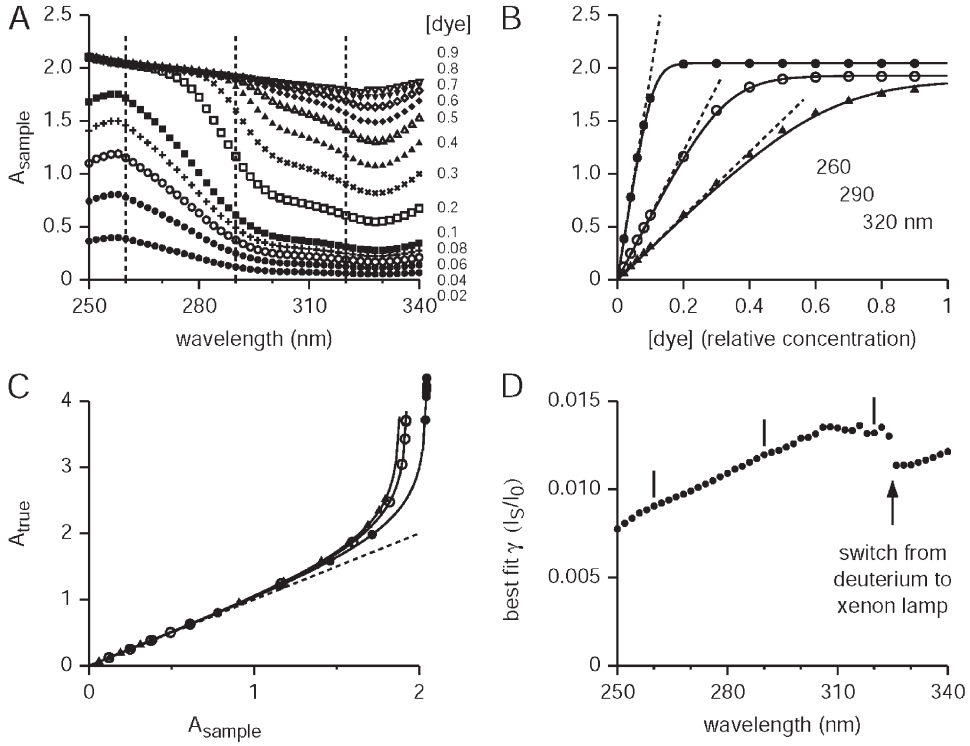

Figure S3. Characterization of the stray light on the absorbance spectra of green dye and illustration of the determination of I_S/I_0 values. (A–D) See text for details.

associated with a muscle sample in this study, A_{true} generally includes a contribution from muscle components and the Ca-free and/or the Ca-bound forms of BAPTA.

Dividing the numerator and denominator in Eq. S20 by I_0 and then substituting in Eq. S21 gives

$$A_{sample} = \log_{10}\left(\frac{1+\gamma}{I/I_0+\gamma}\right) = \log_{10}\left(\frac{1+\gamma}{10^{-A_{true}}+\gamma}\right), \quad \text{(S22)}$$

where

$$\gamma \equiv \frac{I_S}{I_0}. \quad \text{(S23)}$$

The first use of Eq. S22 was to determine γ by measuring A_{sample} at known values of A_{true} using a dye known to obey Beer's law. Fig. S3 A shows 13 absorbance spectra measured at different concentrations of green food–coloring dye, a dye known to obey Beer's law and one of the dyes generally recommended for calibrating spectrophotometers based on this property (e.g., Frings and Broussard, 1979). Each symbol represents a different relative concentration of the dye, as indicated on the right-hand side of A. A solution corresponding to the value 1 was obtained by adding 200 drops of green food coloring (Club House brand purchased in a grocery store) in 100 ml water; the other concentrations were obtained by dilution of this stock solution with water. (A spectrum for the stock solution is not shown because we forgot to do it.) The symbols in Fig. S3 B plot A_{sample} versus [dye] values from the data in A, with each symbol representing a different wavelength, either 260, 290, or 320 nm, as indicated. These wavelengths are also indicated by the vertical dashed lines in A. The dashed lines in B are the expected A_{true} versus $[dye]$ relationships. These lines pass through the points (0, 0) and the point with the lowest dye concentration so that they are given by the linear relationship

$$A_{true}([dye]) = \frac{[dye]}{[dye]_{lowest}} A_{true}([dye]_{lowest}), \quad \text{(S24)}$$

where $[dye]_{lowest}$ is the lowest dye concentration (relative dye concentration = 0.02). Eq. S24 is justified because the errors caused by the stray light are negligible at this lowest concentration, as detailed below, and because the green food–coloring dye is known to obey Beer's law. The solid lines in B are given by Eq. S22 using A_{true} values from Eq. S24 and the least-squares best-fit value of γ (obtained by minimizing the sum of squares of the difference between measured values of A_{sample} and values of A_{sample} predicted with Eq. S22).

Eq. S22 can be rearranged to give

$$A_{true} = A_{sample} + \log_{10}\left(\frac{1}{1+\gamma(1-10^{A_{sample}})}\right). \quad \text{(S25)}$$

Eq. S25 can be used to correct a blank-corrected measured absorbance (A_{sample}) to give the actual absorbance, provided that the value of γ is known. It is noted that A_{true} is always $\geq A_{sample}$ as long as $A_{true} < \infty$. Fig. S3 C shows application of Eq. S25 for the same three sets of data and associated values of γ shown in B. It is seen from these curves that A_{true} starts to noticeably deviate from A_{sample} starting at absorbance values near 1, with the difference between A_{true} and A_{sample} progressively increasing with increasing absorbance values. The curves approach asymptotic values as A_{true} and $[dye]$ approach relatively large values. An asymptotic value is given by

$$A_{sample}([dye] \to \infty) = \log_{10}\left(1+\frac{1}{\gamma}\right),$$

obtained by combining Eq. S23 with Eq. S20 and setting $I = 0$. Based on visual inspection of the curves, it seems reasonable to conclude that the correction procedure is reliable for our spectrophotometer for A_{sample} values up to 1.5–1.8, depending on the wavelength. Although the correction procedure appeared to work for all of the points measured, its reliability is expected to significantly diminish as the asymptotic value for A_{sample} is approached.

Fig. S3 D plots all of the values of γ for the full wavelength range of 250–340 nm used in this study. The vertical line segments mark the value of γ obtained at the wavelengths shown in B and C. There is some deviation in the progressively increasing value of γ with wavelength at the point marked by the arrow. As indicated, this arrow marks the wavelength where the spectrophotometer switches from its deuterium to its xenon lamp. The increasing values of γ with wavelength are likely caused by the fact that light intensity from the deuterium lamp decreases with increasing wavelength in this wavelength range.

In summary, the calibration and correction procedures shown here enabled us to extend the useful wavelength range of our spectrophotometer from a maximum A_{sample} value of ~1 to values approaching 1.5–1.8. Although it was previously well established that green food–coloring dye or related dyes can be used to assess the nonlinearity in spectrophotometers, to our knowledge, this is the first description of how information from such dyes can be used to correct absorbance values thereby extending the useful range of a spectrophotometer.

Section 4: Ca leaching from labware affected Ca standard measurements but should not have affected the $[Ca_T]_{WM}$ results based on Beer's law

Results in this section show that significant differences were often observed between measured and expected values of $[CaB]_S$, and that these differences were caused entirely, or in large part, by Ca leaching from two labware sources. Fig. S4 A plots the measured value of $[CaB]_S$ with no muscle present (Eq. 19b) versus the number of days after making the nominal 1.5-mM $CaCl_2$ solution used for the standard measurements. For the

Ca standard measurements for the results in Fig. S4 A, 9 µl of the nominal 1.5-mM $CaCl_2$ solution was added to a 0.45-ml sample (S_M) to give a nominal (or "expected") increase in [CaB] of 0.03 mM (as elsewhere, this concentration refers to the volume before adding the 9 µl). The nominal 1.5-mM $CaCl_2$ solution was made by multiple dilutions using highly purified water (>18 MΩ-cm) starting with a 0.1-M $CaCl_2$ standard (Fluka/Sigma-Aldrich), and it was stored in a glass scintillation vial at ∽4°C. Despite some scatter in the data, it is clear that measured values of $[CaB]_S$ near the start were close to, but somewhat greater than, the expected value of 0.03 mM, and then the values progressively increased with time, reaching values >33% (>0.04 mM) of the expected value within 120 d. As no other explanation seems plausible, the progressive increase is almost certainly caused by Ca leaching from the glass scintillation vial, increasing the $CaCl_2$ concentration by >33% (i.e., from ∽1.5 to >2.0 mM).

As an example of the scatter in the reported values of $[CaB]_S$ made on one day, the open circles on the right-hand side of Fig. S4 A plot $[CaB]_S$ values obtained with muscle present (Eq. 19a) along with their associated value of $[CaB]_S$ determined without muscle present (shown as a closed circle and plus symbol, the same closed circle and plus symbol that were plotted at 42 d). This result shows that there was significant scatter in the $[CaB]_S$ values even though they were expected to all have the same value. Similar variability in $[CaB]_S$ was observed in all of the experiments in which glass Pasteur pipettes were used to mix the added 9 µl of Ca standard with the A_M solution to give the A_S aliquot. (This was the mixing procedure used for all of the experiments in this Methods and Approaches article except for a couple of experiments performed after the discovery of this problem.) As described next, Ca was later found to leach from Pasteur pipettes during the mixing process, a source of Ca responsible, at least in part, for the variability of $[CaB]_S$ values.

Fig. S4 B plots the BAPTA absorbance at 292 nm of the usual measurement solution versus the number of exchanges of the solution with a Pasteur pipette. A single exchange consists of taking up almost all of the 0.45 ml of solution into the pipette and expelling it back into the cuvette. (Several exchanges of this type were used to convectively mix in the cuvette added EGTA so-

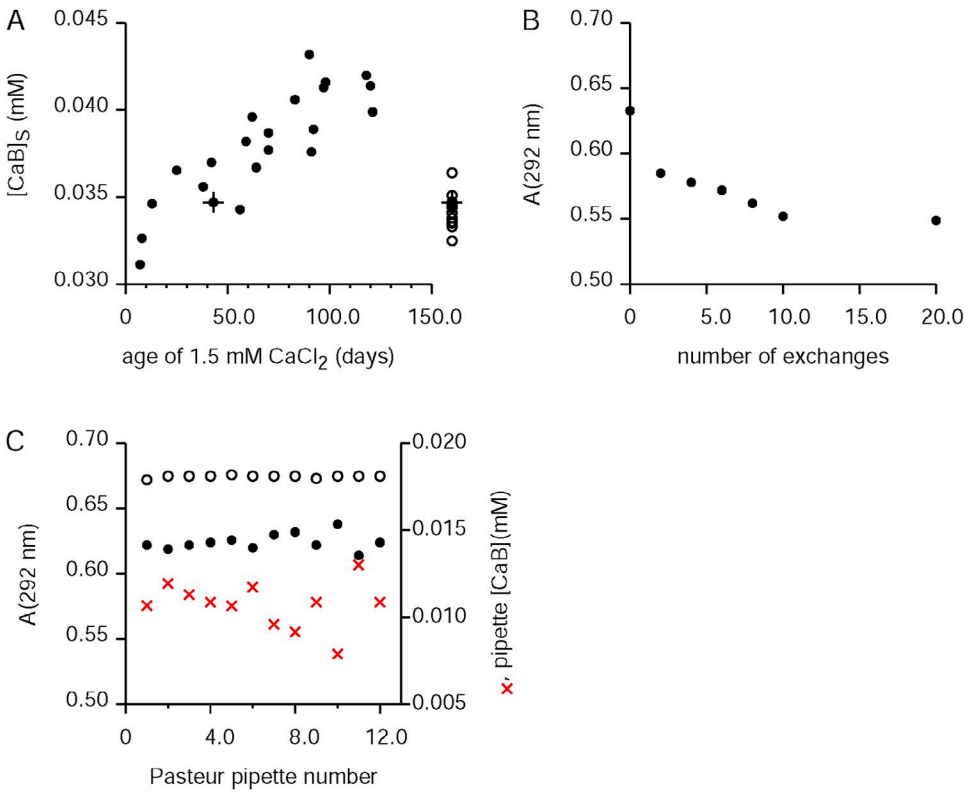

Figure S4. Ca leaching from labware used for Ca standard measurements. (A) The amount of Ca added with the Ca standard increased with time, an effect attributed to Ca leaching from the glass scintillation vial in which the 1.5-mM Ca standard was stored. (B) The decrease in BAPTA absorbance at 292 nm (increase in CaBAPTA concentration) versus the number of exchanges of the solution in the cuvette. An exchange is defined as taking the solution up into a glass Pasteur pipette and returning it to the cuvette. Several (two to four) such "exchanges" were generally used to mix added components (EGTA or Ca) into the cuvette, although nothing was added in this case. The decreased absorbance is attributable to Ca leaching from the Pasteur pipette. (C) The amount of Ca leached varies from pipette to pipette. See text for additional details.

lution, for the A_0 and S_0 aliquots, or added Ca solution, for the A_S, S_S, A_∞, and S_∞ aliquots.) There was a clear, progressive decrease in absorbance attributable to an increase in Ca attributable to Ca leaching from the Pasteur pipette, as it was made of soda-lime glass, which contains Ca.

The results in Fig. S4 C show tests of 12 different Pasteur pipettes to assess whether the amount of Ca leaching varies from one pipette to another. The open circles in Fig. S4 C show absorbance values of the usual measurement solution. The closed circles show the absorbance after two exchanges with the Pasteur pipette. The red X symbols plot the [CaB] value determined from the absorbance change (see Eq. 19b). The scatter in red X-symbol data can be explained by variation in the amount of Ca leached from the different Pasteur pipettes. The range of this scatter is similar to that seen with the open and closed symbols in Fig. S4 A (for the closed symbols, the scatter is not associated with the progressive increase in $[CaB]_S$), so it is likely that these variations are also caused by different degrees of Ca leaching from Pasteur pipettes.

It is noted that the average value for [CaB] caused by Ca leaching from the pipettes in Fig. S4 C was >0.01

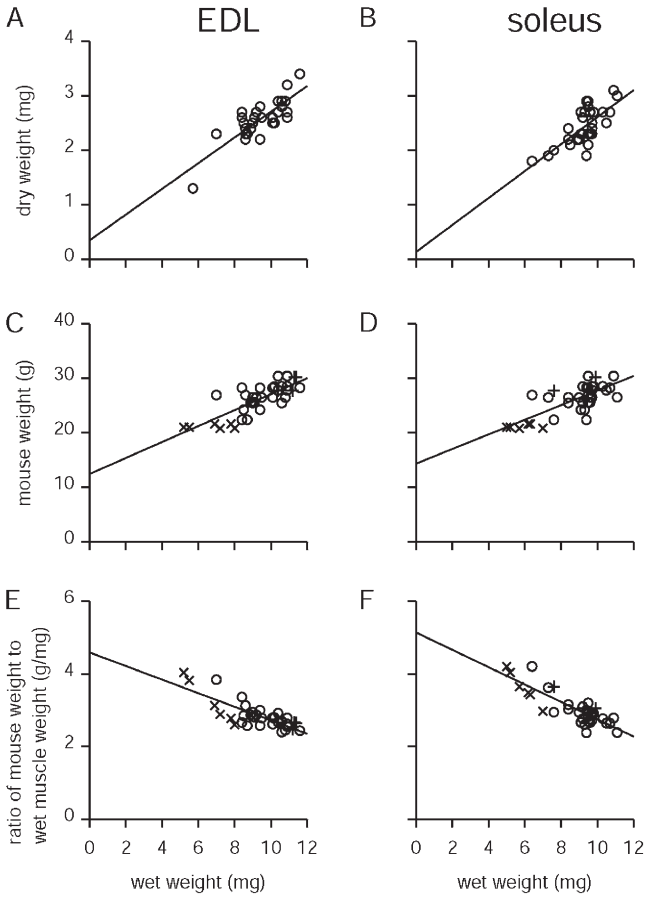

Figure S5. Plots versus wet muscle weights of dry muscle weight, whole mouse weight, and the ratio of whole mouse weight to wet muscle weight. As indicated, the panels on the left and right sides were obtained with mouse EDL and soleus muscles, respectively. The open circles in all six panels were taken from the same set of C57BL/6 mice ordered at the same time. The + and × symbols in C–F were from two other sets of mice plotted with the same symbols in Fig. 6. (See the legend of Fig. 6 for details about the mice used for these two sets.) All panels plot some variable with respect to the wet weight of the muscle on the abscissa. The top (A and B), middle (C and D), and bottom panels (E and F) plot, respectively, dry muscle weight, weight of the mouse from which the muscles were taken, and the ratio of mouse weight to wet muscle weight. Each panel shows the least-squares best-fit line to the data. The slopes (intercepts; p-values) of these lines are: (A) 0.236 mg/mg (0.347 mg; $P < 0.0001$), (B) 0.247 mg/mg (0.133 mg; $P < 0.0001$), (C) 1.464 g/mg (12.43 g; $P = 0.0054$, (D) 1.341 g/mg (14.32 g; $P = 0.0263$), (E) -0.187 g/mg^2 (4.59 g/mg; $P < 0.0001$), and (F) -0.239 g/mg^2 (5.14 g/mg; $P < 0.0001$). The average values (SEM; *n* values) for the variable plotted on the ordinates for the six panels are: (A) 2.57 mg (0.24 mg; 29), (B) 2.44 mg (0.06 mg; 32), (C) 26.1 g (0.5 g; 36), (D) 26.2 g (0.5 g; 38), (E) 2.85 g/mg (0.06 g/mg; 36), and (F) 3.03 g/mg (0.07 g/mg; 38). For the wet muscle weights (abscissa values) in A and B, the average values (SEM; *n* values) for EDL and soleus muscles were 9.43 mg (0.24 mg; 29) and 9.33 mg (0.18 mg; 32), respectively. For the wet muscle weights (abscissa values) in C and D (and E and F), the average values (SEM; *n* values) for EDL and soleus muscles were 9.32 mg (0.27 mg; 36) and 8.82 mg (0.26 mg; 38), respectively. The average ratios (SEM; *n* values) of dry to wet muscle weights for EDL and soleus muscles were, respectively, 0.242 (0.016; 29) and 0.262 (0.004; 32) mg/mg.

mM, which is about the magnitude of the largest unexpected increase in $[CaB]_S$ in A. This >0.01-mM magnitude is not readily reconciled with the early results in Fig. S4 A showing that the measured values of $[CaB]_S$ were close to the expected value of 0.03 mM, unless there was some difference in the Pasteur pipettes used for the experiments in A and C. This was likely the case, as the Pasteur pipettes used in C were purchased after all the data in A was obtained.

Fortunately, the problem of Ca leaching from Pasteur pipettes should not have impacted the main results in this study, as explained here. As noted above, because of this problem, the value of $[B_T]$ needed for obtaining the amount of Ca in a muscle sample was determined with the approach based on Beer's law (Eq. 6) instead of the approach based on the Ca standard (Eq. 8). Very importantly, the A_m and S_m aliquots did not require mixing, so they had no contact with a Pasteur pipette. Pasteur pipettes were used for mixing the A_0 and S_0 aliquots, but these involved adding excess EGTA, which would have bound essentially all of the Ca leached from the Pasteur pipette. In the case of the A_∞ and S_∞ aliquots, the extra Ca would not have been a problem, as the aim of these aliquots was to add excess Ca so that essentially all of the BAPTA was in the Ca-bound form. For the purpose in the article of comparing $A_M - A_S$ with $S_M - S_S$ to assess whether muscle affects the ability of BAPTA to detect Ca, the fact that Ca leached from the pipette should not be important (other than the added random variability) because samples with and without muscle were treated in the same way, including mixing of the A_S and S_S samples with Pasteur pipettes.

Section 5a: The inverse relationship between $[Ca_T]_{WM}$ and wet muscle weight is not caused by differences in fractional water content

As noted with Fig. 6, $[Ca_T]_{WM}$ (units of millimoles of Ca per kilogram of wet muscle weight) approximately doubled when wet muscle weight was halved over most of the range of muscle weights (from 12 to 6 mg) for both mouse EDL and soleus muscle samples. This means that the total Ca content of the muscle (product of $[Ca_T]_{WM}$ and wet muscle weight) did not change much. One possible explanation is that all of the muscle samples had about the same amount of solids (protein, lipids, and any other nonaqueous components), so that the greater wet weights were caused by greater fractional water contents in the muscle samples, a result of excess extracellular and/or intracellular water fractions, perhaps caused by the way the muscle samples were processed. For example, differences in the extracellular fractional water content could be caused by differences in the extent that water is removed from the muscle during the step of blotting the muscle sample on tissue just before weighing it, although such differences are expected to be minor. Because this explanation means dry muscle weight would remain constant and therefore not depend on wet muscle weight, the experiments in this section were performed to assess the possibility of variability in the fractional water content by adding dry muscle weight to the usual measurements.

The results in this section were from experiments performed in the usual way and with the same type and age range (4–6 mo) of the mice used in Fig. 6 (A and C), except that the muscle samples were dried. After measuring the wet muscle weight in the usual way, muscle samples were placed on squares of aluminum foil (⌣2-cm sides) and dried in an oven at 70°C for 42 h. A and B in Fig. S5 plot the dried muscle weights versus wet muscle weights for EDL and soleus muscle samples, respectively. The least-squares best-fit lines for both muscle types have y intercepts close to zero, indicating that the dry muscle weight is approximately proportional to wet muscle weight. If the range of muscle weights was totally attributable to differences in the fractional water content with no change in the total mass of proteins and other solids, the fitted lines in A and B would have been horizontal. This was not the case, as the slopes of the fitted lines were significantly different than zero (see legend to Fig. S5). Moreover, the y intercepts are very close to zero, indicating a proportional relationship between dry and wet muscle weights. This proportionality means that the inverse relationships between $[Ca_T]_{WM}$ and wet muscle weight in Fig. 6 were not caused by differences in the fractional water content.

Section 5b: Muscle weight versus mouse weight: Smaller muscles need to propel fractionally greater mouse body weights

C and D in Fig. S5 plot the weight of the mice from which the EDL and soleus muscles, respectively, were taken versus wet muscle weight. The positive slopes were again significantly different than zero, indicating that a lighter muscle weight tended to be associated with a lighter mouse. The positive y intercepts indicate that the muscle weights are not proportional to mouse weights; rather, the muscle weights vary over a fractionally greater range than the mouse weights.

E and F in Fig. S5 plot the ratio of mouse weight to wet muscle weight versus wet muscle weight for the same data points shown in C and D, respectively. Again, the least-squares best-fit slopes are significantly different than zero. These results support the explanation for the inverse relationship between $[Ca_T]_{WM}$ versus muscle weight given with Fig. 6 in the main text. The muscle fibers in the smaller muscles would tend to have a higher relative workload because of their greater mouse weight to muscle weight ratio and that some, as yet unknown, mechanism sensing this greater workload somehow increases the concentration of total Ca in the muscle fibers to produce a greater specific force.

The lines in E and F in Fig. S5 were used to generate the linear scales at the top of the panels in Fig. 6 in the main text. The reason for this is that mouse weights were not measured for most of the points in Fig. 6, with the important exception of the data points plotted with + and × symbols in B and D of Fig. 6 (plotted with the same symbols in Fig. S5, C–F), as the values of *R* and muscle weights associated with these points span most of the ranges for these parameters. The linear relationships are expected to apply to the data in Fig. 6, even though more than half of the *R* versus muscle weight data points used for these relationships (the open circle symbols) were from a different set of mice. As seen in E and F of Fig. S5, the least-squares best-fit lines provide a good fit to all of the *R* versus muscle weight data. Moreover, the same relationship between *R* and muscle weight would be expected, as the muscle strains were the same or very similar, and the age of the mice were in the same range, 3–6 mo.

Section 5c: Apparent nonreproducibility in $[Ca_T]_{WM}$ results is attributable to contamination of the muscle samples by aluminum

A and B in Fig. S6 plot $[Ca_T]_{WM}$ versus wet muscle weight for most of the muscles reported in Fig. S5 (not all of the muscles were analyzed). As in Fig. 6 in the main text, the least-squares best-fit lines again show marked inverse relationships between $[Ca_T]_{WM}$ and muscle weight. However, as described here, there were problems with the set of $[Ca_T]_{WM}$ values shown in these panels that are likely caused by contamination with aluminum from the aluminum foil used to dry the muscle. The solid line in A and B show the least-squares best-fit line to the plotted points. The hashed line in A and B shows the least-squares best-fit line to the data in Fig. 6 (A and C, respectively). To help with the comparison, these best-fit lines and the data from Fig. 6 (A and C) are also plotted in C and D, respectively, of Fig. S6. Despite the fact that the sets of mice used for the top and bottom panels were from the same strain (C57BL/6) and were within the same age range (4–6 mo), the results for the two sets were significantly different. The main differences are: (a) the slopes of the fitted lines (see legend to Fig. S6) for the points in the top panels are three to four times greater than those in the bottom panels; (b) the average values (see legend to Fig. S6) are 61 and 93% greater for the EDL and soleus muscles data, respectively; and (c) the data points are much more scattered. As seen in Fig. 6 (B and D), the $[Ca_T]_{WM}$ versus muscle weight results from several different sets

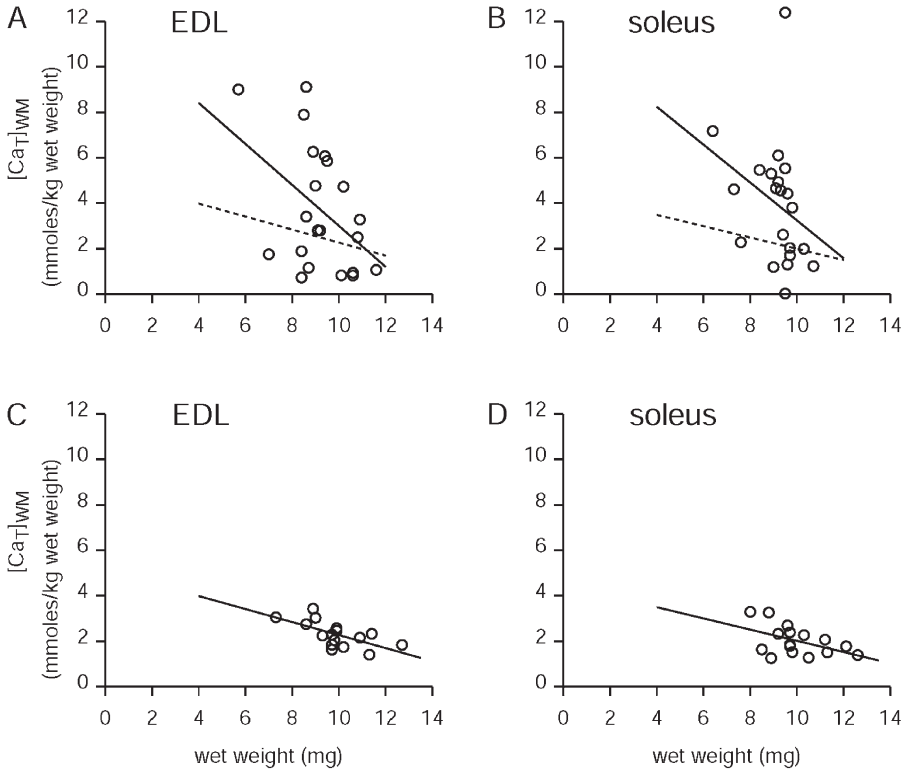

Figure S6. Plots of $[Ca_T]_{WM}$ values versus wet muscle weights for EDL (A and C) and soleus muscles (B and D). The results in A and B are from the set of mice used for the experiments in Section 5. The results in C and D are from the set of results plotted in Fig. 6 (A and C, respectively). The solid line in each panel shows the least-squares best-fit line to the data. The slopes in units of millimoles/kilogram wet weight per milligram wet weight (intercepts in units of millimoles/kilogram wet weight) of these lines are: (A) −0.902 (12.02), (B) −0.834 (11.58), (C) −0.287 (5.13), and (D) −0.247 (4.48). The average values of $[Ca_T]_{WM}$ for the four panels are: (A) 3.70, (B) 3.97, (C) 2.30, and 2.06 mmoles/kg wet weight. See text for additional details.

of muscles were reasonably well described by the same fitted line, indicating that the results were reproducible. Because the results with the dried muscle samples in Fig. S6 (A and B) are markedly different, this indicates that the BAPTA method is either nonreproducible or that something else occurred with these experiments. Results given next show that the $[Ca_T]_{WM}$ values with the dried muscles are unreliable. Results discussed afterward indicate that the greater apparent $[Ca_T]_{WM}$ values are very likely the result of contamination by aluminum ions (Al^{3+}). Collectively, these results mean that the discrepancies between the top and bottom panels in Fig. S6 are not caused by nonreproducibility with the BAPTA method.

Each point in Fig. S7 plots $[Ca_T]_{WM}$ for a muscle taken from the right side of a mouse versus $[Ca_T]_{WM}$ for the muscle sample taken from the left side of the same mouse (i.e., paired samples). A and C were obtained with EDL muscles, and B and D were obtained with soleus muscles. The muscles for the top panels (A and B) were not dried, whereas those for the bottom panels (C and D) were dried on aluminum foil. The lines in each panel correspond to the situation that the left- and right-side values exactly match (i.e., they have slopes of 1 and intercepts of 0). The data in A and the corresponding data for soleus muscles from the same mice shown in B are from the set of results shown in Fig. 6, also shown above in Fig. S6 (C and D). Although there is some deviation from equality, the data without drying do approach the expectation of equality between $[Ca_T]_{WM}$ between paired left and right muscle samples. In contrast to the expectation of approximately equal values for left and right muscle samples from the same mouse, the data obtained with drying on aluminum foil in the bottom panels are very scattered. (Note the greater than twofold difference in the scales in the bottom vs. top panels in Fig. S7, so that the discrepancy is even greater than it appears by a visual comparison between the bottom and top panels.) The lack of equality between the $[Ca_T]_{WM}$ values for the paired dried muscle samples is considered as evidence that the results are unreliable.

As noted above, the experiments with the dried muscle samples were performed as those in Fig. 6 were, with the exception of the drying process. The only difference that we can think of that could reasonably explain the results is that Al^{3+} from the aluminum foil leached into the muscle samples during the drying process. The possibility that Al^{3+} could interact with BAPTA was assessed by adding Al^{3+} in the same way used for Ca standard measurements (9-µl additions of 45 mM aluminum sulfate introduced into 0.45-ml samples of the usual measurement solution, resulting in an addition of 0.9 mM of Al^{3+}). This maneuver resulted in an initial decrease in BAPTA absorbance measured at 292 nm (de-

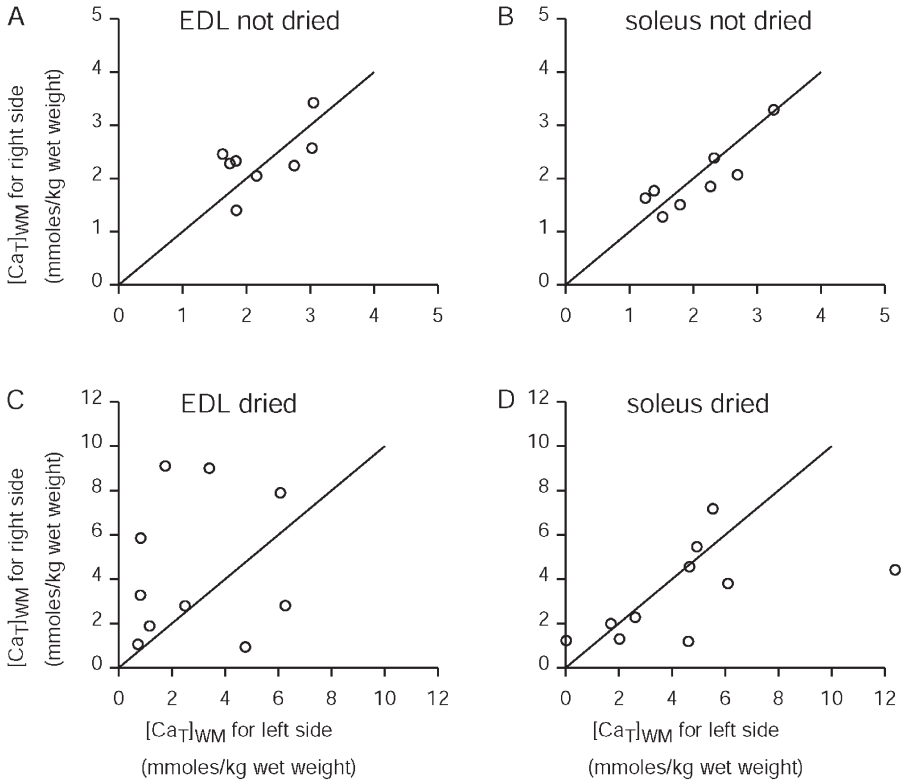

Figure S7. Plots of $[Ca_T]_{WM}$ values from muscles taken from the right side of a mouse versus the left side. A and B are from the results for EDL and soleus muscles, respectively, in Fig. 6 (A and B) in the main text. C and D are from EDL and soleus muscles, respectively, from the set of mice used for Section 5. See text for additional details.

noted "A(292)") to significantly less than half of the initial value. Curiously, A(292) increased approximately exponentially, approaching a steady level within a few minutes that was ∼10% less than the initial value of A(292) before adding Al^{3+}. Subsequent additions of the same amount of Al^{3+} displayed decreases in A(292) of about the same magnitude (by ∼10%) as that produced in the steady level with the first 9-µl addition of aluminum sulfate, although without the initial, much larger decrease in A(292) and subsequent recovery. We do not have a simple explanation for the initial decrease and subsequent recovery seen only with the first 9-µl addition, although it may have something to do with the precipitation of Al^{3+} as aluminum hydroxide known to occur at neutral and basic pH levels. If the value of the initial large decrease in A(292) to less than half of the initial was the correct value to use for the purpose of estimating the K_d for Al^{3+} binding to BAPTA, a very rough estimate for this K_d would be near, although somewhat <1 mM. If the steady levels are the appropriate values to use, the results above give a very rough estimate for the K_d of ∼5 mM (5 mM is the approximate concentration needed to reduce the steady value of A(292) to about half its initial value). As with Ca binding, adding EGTA reverses the decrease in BAPTA absorbance. Because the addition of 1 mM EGTA (9-µl addition of 50 mM EGTA into 0.45-ml cuvette) completely or nearly completely reverses the decrease in A(292) by 0.9 mM aluminum sulfate, these preliminary results indicate that EGTA binds Al^{3+} with high affinity. In regards to the initial aim of these experiments, the main conclusion from these preliminary results is that Al^{3+} does appear to bind to BAPTA, reducing its absorbance, and EGTA competes the Al^{3+} off BAPTA. Therefore, contamination by Al^{3+} could be interpreted as Ca^{2+} binding with the BAPTA method. We conclude with near certainty that this is what occurred with the dried muscle samples caused by leaching from the aluminum foil used in the drying procedure. Different degrees of leaching would explain the greater scatter in the data compared with the earlier results (top vs. bottom panels in Fig. S6) and the marked non-equality of $[Ca_T]_{WM}$ values from paired left and right muscles (bottom panels in Fig. S7). The three- to fourfold steeper slopes of the least-squares best-fit lines in the top panels in Fig. S6, giving the appearance of more pronounced inverse relationships between $[Ca_T]_{WM}$ and muscle weight, could be explained by greater Al^{3+} leaching into smaller muscles as a result of their greater surface to volume ratios.

Section 6: Possible explanation for two outlier points and criterion used to reject them

Two $[Ca_T]_{WM}$ data points, termed outliers, were considered unreliable and were rejected because their values were significantly out of the range of the other values in their set, and because there is a reasonable explanation for why this might have occurred (of the total number of points in this study from 148, 31, and 16 from, respectively, mouse, frog, and rat muscle samples, only one point from the mouse and one point from the frog muscle samples were rejected). The criterion for rejecting the points was that their values were greater than three standard deviations than the mean of the remaining points in their group. There was no reason to suspect any bimodal distribution in the data, as sets of data had normal distributions as assessed by approximately linear normal probability plots (not depicted; for the sets with the outlier points, their distributions also appear normal without the outlier points). Neither of the outliers was from the main set of control muscles, and each of these points is discussed in the main text. The two outliers were not included in the final averages for the dataset to which they belonged (one point is in Fig. 7 A, and the other is from a frog muscle exposed to normal Ringer's solution for 1 h). Part of the justification for rejecting these points from the final averages is that it is quite possible that they occurred because of experimental error as explained here. For a given muscle sample, the four aliquots were measured in the order A_M, A_0, A_S, and A_∞, and similarly for the background solution measurements, S_M, S_0, S_S, and S_∞. As a result, the first measurement in the next sample (A_M or S_M) came after the sample with excess Ca from the preceding sample. Although care was taken to thoroughly rinse the cuvette before introducing a new aliquot, it is possible that a small amount of the high Ca solution in the A_∞ (or S_∞) aliquot was not removed, thereby increasing the Ca in the following A_M (or S_M) aliquot.

Section 7: Predictions of the degrees to which $[Ca_T]_{WM}$ would be reduced by CSQ KO

To interpret the results with CSQ knocked out in EDL muscle, it is helpful to first estimate the total Ca present in normal muscle minus that bound to CSQ. This estimate, to follow, gives the predicted value of $[Ca_T]_{WM}$ with CSQ KO assuming that the only effect of the KO was to remove the Ca component bound to CSQ. For this purpose, the SR component of total Ca ($[Ca_T]_{SR}$) for Eqs. 23a in the main text is separated into free Ca^{2+} ($[Ca^{2+}]_{SR}$) and bound Ca ($[CaBound]_{SR}$), as given by the following equations:

$$[Ca_T]_{WM} = [Ca_T]_{EC} + [Ca_T]_{NonSR} + [Ca^{2+}]_{SR} + [CaBound]_{SR}. \quad \text{(S26a)}$$

Similar to Eqs. 23b–23d in the main text, this relationship in fractional terms is given by

$$1.0 = f_{EC} + f_{NonSR} + f_{SR\_free} + f_{SR\_bound}. \quad \text{(S26b)}$$

$$\text{EDL muscle: } 1.0 = 0.11 + 0.12 + 0.026 + 0.744 \quad \text{(S26c)}$$

$$\text{soleus muscle: } 1.0 = 0.11 + 0.02 + 0.030 + 0.840 \quad \text{(S26d)}$$

As with Eqs. 23c and 23d, Eqs. S26c and S26d give estimated values for the fractions of $[Ca_T]_{WM}$ associated with the different components in EDL and soleus muscles, respectively. The sums of f_{SR_free} and f_{SR_bound} are 0.77 and 0.87 for Eqs. S26c and S26d, respectively, the same values given for f_{SR} in Eqs. 23c and 23d, respectively. The ratios of f_{SR_free} and f_{SR_bound} were determined from the estimated ratio of 1 free Ca^{2+} ion for 28 bound Ca atoms in the SR (Fénelon et al., 2012). As covered in the Introduction of the main text, results of Fénelon et al. (2012) with frog twitch muscle indicate that at least 80% of the Ca in the SR at rest is bound to CSQ, although this percentage would be closer to 97% if CSQ were the only source of bound Ca in the SR CSQ. (97% is from the ratio of 1:28 for free Ca^{2+} to bound Ca.) Based on results with mammalian skinned fibers, Murphy et al. (2009) concluded that Ca-binding sites on CSQ account for all of the maximal bound Ca in the SR, indicating that Ca-binding sites on CSQ are, in fact, the only nonnegligible sites for bound Ca in the SR. With the bound form of Ca in the SR all attributed to CSQ and with the above assumptions, CSQ KO is predicted to reduce $[Ca_T]_{WM}$ to 0.256 (1 − 0.744) and 0.160 (1 − 0.840), respectively, of the values for EDL and soleus muscles from WT mice.

REFERENCES

Fénelon, K., C.R.H. Lamboley, N. Carrier, and P.C. Pape. 2012. Calcium buffering properties of sarcoplasmic reticulum and calcium-induced Ca^{2+} release during the quasi-steady level of release in twitch fibers from frog skeletal muscle. *J. Gen. Physiol.* 140:403–419. http://dx.doi.org/10.1085/jgp.201110730

Frings, C.S., and L.A. Broussard. 1979. Calibration and monitoring of spectrometers and spectrophotometers. *Clin. Chem.* 25:1013–1017.

Godt, R.E., and B.D. Lindley. 1982. Influence of temperature upon contractile activation and isometric force production in mechanically skinned muscle fibers of the frog. *J. Gen. Physiol.* 80:279–297. http://dx.doi.org/10.1085/jgp.80.2.279

Harrison, S.M., and D.M. Bers. 1987. The effect of temperature and ionic strength on the apparent Ca-affinity of EGTA and the analogous Ca-chelators BAPTA and dibromo-BAPTA. *Biochim. Biophys. Acta.* 925:133–143. http://dx.doi.org/10.1016/0304-4165(87)90102-4

Murphy, R.M., N.T. Larkins, J.P. Mollica, N.A. Beard, and G.D. Lamb. 2009. Calsequestrin content and SERCA determine normal and maximal Ca^{2+} storage levels in sarcoplasmic reticulum of fast- and slow-twitch fibres of rat. *J. Physiol.* 587:443–460. http://dx.doi.org/10.1113/jphysiol.2008.163162

Pape, P.C., D.-S. Jong, and W.K. Chandler. 1995. Calcium release and its voltage dependence in frog cut muscle fibers equilibrated with 20 mM EGTA. *J. Gen. Physiol.* 106:259–336. http://dx.doi.org/10.1085/jgp.106.2.259

Tsien, R.Y. 1980. New calcium indicators and buffers with high selectivity against magnesium and protons: design, synthesis, and properties of prototype structures. *Biochemistry.* 19:2396–2404. http://dx.doi.org/10.1021/bi00552a018